Electronic Supplementary Material (ESI) for Nanoscale.

Supplemental information

Controlling Molecular Ordering in Solution-State Conjugated Polymers

Jiahua Zhu[1], Youngkyu Han[2], Rajeev Kumar[1,3], Youjun He[1], Kunlun Hong[1], Peter V. Bonnesen[1], Bobby G. Sumpter[1,3], Sean C. Smith[4], Gregory S. Smith[2], Ilia N. Ivanov[1*] and Changwoo Do[2*]

1. Center for Nanophase Materials Sciences, Oak Ridge National Laboratory, Oak ridge, TN 37831, USA. 2. Biology and Soft Matter Division, Oak Ridge National Laboratory, Oak ridge, TN 37831, USA. 3. Computer Science and Mathematics Division, Oak Ridge National Laboratory, Oak ridge, TN 37831, USA. 4. School of Chemistry&Molecular Biosciences, University of Queensland, Brisbane, St Lucia, QLD 4072, Australia.

Email: ivanovin@ornl.gov and doc1@ornl.gov

Table of Contents

1. Theoretical predictions

1.1 Self-consistent field theory (SCFT) simulations

We have used SCFT for polymers to develop an understanding of partitioning of the P3EOT chains in the domains formed by $C_{12}E_5$ and water. The SCFT has been very well documented in the literature. [1,2,3] In the following, we only describe the mesoscopic model and the numerical procedure.

Due to the fact that $C_{12}E_5$ is a short diblock copolymer containing hydrophilic ethylene oxide moieties and a hydrophobic methylene block, we have modeled each $C_{12}E_5$ chain by a continuous curve of length $(N_A + N_B)$ b, where N_A =10 and N_B =10 are the numbers of Kuhn segments of type A and B, respectively, each of length b. For comparisons with the experimental investigations done in this work, A represents the ethylene oxide and B represents the methylene group. Within the SCFT, the chemical nature of different monomers appears through the Flory's parameter, $\boldsymbol{\chi}_{AB}$, characterizing short-range interactions between the two kinds of monomers. Typically, $\chi_{AB} = z[\varepsilon_{AB}-0.5(\varepsilon_{AA}+\varepsilon_{BB})]/k_BT$ decreases with an increase in temperature (T) [1], where z is the coordination number and ε_{ij} is the interaction energy between i and j and k_B is the Boltzmann constant. P3EOT is modeled by a flexible homopolymer (H) of length N_H b and N_H is taken to be 20. Water is treated as a small neutral molecular solvent, which interacts with the diblock and homopolymer by three parameters, χ_{AS}, χ_{BS} and χ_{HS}, representing interactions between A-solvent, B-solvent, and H-solvent pairs, respectively.

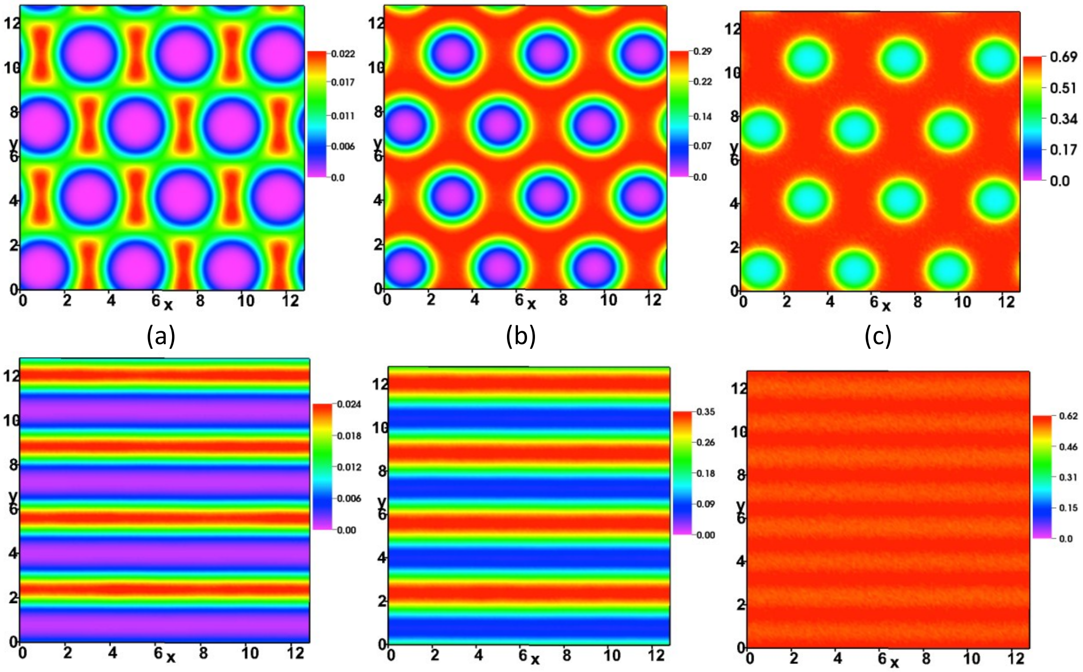

(a) (b) (c)

(d) (e) (f)

Figure S1. **Component distribution in a ternary system consisting of P3EOT, $C_{12}E_5$ and water.** Predictions from the self-consistent field theory (SCFT) for the volume fraction profiles of different components in ternary mixtures of P3EOT (1% by volume), $C_{12}E_5$ (40%) and water (59 %). Top and bottom panels correspond to low (corresponding to $\chi_{AB} = \chi_{BH} = 1.5$, $\chi_{AS} = \chi_{HS} = 0.01$ and $\chi_{BS} = 1.0$) and high temperatures (corresponding to $\chi_{AB} = \chi_{BH} = 1.5$, $\chi_{AS} = \chi_{HS} = 0.01$ and $\chi_{BS} = 0.01$) exhibiting hexagonal and lamellar packing of $C_{12}E_5$, in agreement with the experiments. The effect of temperature is modeled through temperature-dependent polymer-solvent chi parameter. Panels (a) and (d) represent volume fraction profiles of the P3EOT; (b) and (e) represent ethyleneglycol monomers in the $C_{12}E_5$; (c) and (f) represent volume fraction of water at the low and high temperature, respectively. From (a) and (d), it is clear that the P3EOT resides in the middle of the hydrophilic domain (i.e., domain containing ethylene glycol from the $C_{12}E_5$) to minimize contacts with the hydrophobic component. Note that each dimension of the simulation box is in units of radius of gyration of a Gaussian chain of the same length as the $C_{12}E_5$ molecule.

From the Hamiltonian of the system describing the short-range interactions and Gaussian chain elasticity terms along with local incompressibility constraint, field theoretical transformations [1,2,3] can be used to construct a field theory. Using the saddle-point approximation, which is equivalent to the mean-field theory, we can alleviate the computational cost of sampling the full statistical mechanical field theory. The approximation leads to a set of non-linear equations, which need to be solved self-consistently using iterative methods. In this work, we have solved these equations using the iterative scheme presented by Sides and Fredrickson. [4] Starting from an initial guess generated by random numbers, the non-linear equations are solved and the free energy of the final structure is calculated. Following the experimental investigations, in this work, we have focused on a ternary mixture of P3EOT (1%

by volume), $C_{12}E_5$ (40%) and water (59 %). Variation of temperature is equivalent to changing χ_{AB}, χ_{AH}, χ_{BH}, χ_{AS}, χ_{BS} and χ_{HS}. In order to understand the partitioning of P3EOT in the domains formed by $C_{12}E_5$ and water, one can vary the six χ parameters. In this work, we have used the fact that the P3EOT has ethylene oxide groups on the side chains and assumed that interaction of each monomer in the P3EOT with other components is similar to each ethylene oxide group in $C_{12}E_5$. The assumption leads to $\chi_{AH} = 0$, $\chi_{AB} = \chi_{BH}$ and $\chi_{AS} = \chi_{HS}$ and there are three independent **χ** parameters. We have varied these three χ parameters (i.e., $\chi_{AB} = \chi_{BH}$, $\chi_{AS} = \chi_{HS}$ and χ_{BS}) to study self-assembly of the ternary mixture. In choosing the χ parameters, we have used criterion [5] for good and poor solvent leading to lower and higher χ values than 0.5, respectively. Also, due to inverse temperature dependence of the χ parameters, their higher values correspond to lower temperatures. For studying partitioning of P3EOT with a change of temperature, we have varied the $\chi_{AS} = \chi_{HS}$ and χ_{BS} parameters, while keeping $\chi_{AB} = \chi_{BH}$ fixed. Results of two such calculations are shown in **Figure S1**.

1.2 Conformational transition of polymer from coiled chain to rod-like chain.

In order to study changes in conformational characteristics of chains during isotropic to nematic transition resulting from the changes in temperature, we use a theory for wormlike chains interacting with each other by Maier-Saupe interaction potential [3,6]. Details of the theory are presented in Ref. 6. In particular, we have used Eq. 5.3 in Ref. 6 written as the ratio of mean square end-to-end distance ($<R_z^2>$) of the chains along the nematic director (taken to be along z-axis) to that of the rods ($=L^2$) of the same contour length ($=L$). Explicitly, the ratio is given by:

$$\frac{< R_z^2 >}{L^2} = \frac{2}{(\lambda_1 - \lambda_0)L}\left[1 + \frac{1}{(\lambda_1 - \lambda_0)L}\left(e^{-(\lambda_1 - \lambda_0)L} - 1\right)\right]\frac{3}{4}\left[\int_{-1}^{1} dx\, Sp_0(x)\, P_1(x) Sp_1(x)\right]^2$$

where $Sp_0(x)$ and $Sp_1(x)$ are the spheroidal functions of order zero and one, respectively, and depend on the Maier-Saupe interaction parameter, $\Delta^2 < 0$, in the notation of Ref. 6. λ_0 and λ_1 are Eigenvalues of the spheroidal wave equation of order zero and one, respectively and depend on $\Delta^2 < 0$. Furthermore, $P_1(x)$ is the Legendre polynomial of order one. We have computed the right hand side of the above equation for different values of L and Δ^2. For these calculations, dimensionless contour length is defined by $\overline{L} = L/2\beta\varepsilon$, where ε characterizes the elastic modulus or the bending strength of the chains, and $\beta = 1/k_B T$. Results for $\overline{L} = 1$ are shown in Figure S2. Qualitatively, similar behavior is seen for higher values of $\overline{L}$, where transition from coil to rod-like conformation is predicted by the theory.

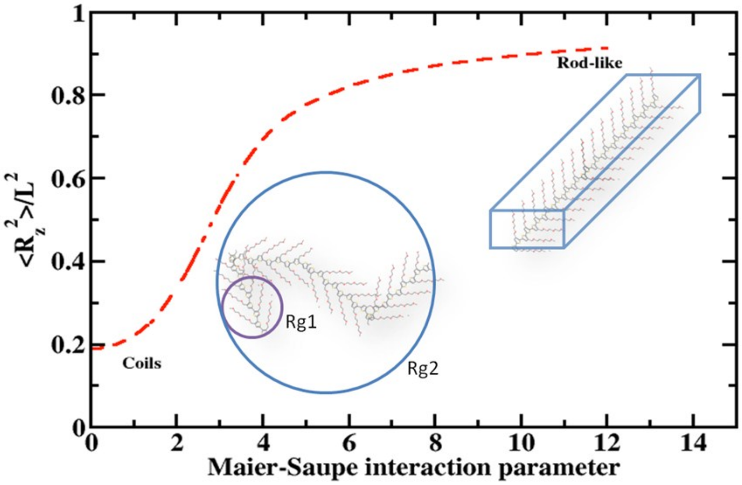

Figure S2. Theoretical prediction[6] for the mean square end-to-end distance of wormlike chains along the director (taken to be along z-axis in this figure) as a function of Maier-Saupe interaction parameter, $|\Delta|$. Here, L is the polymer chain length and it is shown that as a result of an increase in the interaction parameter, chain conformations change from coils to rod-like. Noting that the interaction parameter is dependent on temperature, qualitatively similar behavior is observed in the SAXS experiments.

2. Synthesis of poly(3-(2-(2-(2-methoxyethoxy)ethoxy)ethoxy)methylthiophene)

The water-soluble polythiophene derivative was synthesized using Kumada catalyst transfer polymerization as outlined in **Scheme 1**. [12] The polymer was purified by soxhlet extraction using methanol, hexanes, and tetrahydrofuran (THF). The fraction used in the present work was from the THF soluble portion. The polymer was characterized by 1H-NMR in chloroform-d using a Varian 500 MHz NMR spectrometer, and gel permeation chromatography (GPC) with a Waters 2695 pump system (equipped with Waters 2414 RI and 2996 UV detectors) and THF as the mobile phase (1 mL/min). For all spectroscopic measurements, the polymers were dissolved in deionized water, and fluorescence cuvettes with a 1 cm path length were used. The regioregularity was 97% as measured by 1H-NMR, and its number average molecular weight and polydispersity were Mn=12.3 kg/mol (related to polystyrene standard) and 1.13, respectively.

Degree of polymerization of P3EOT chains at Mw of 12.3k is n = 48. Multiplied by the length of a thiophene repeat unit of 0.4nm, the length of a fully-extended P3EOT chain is estimated to be around 20nm.

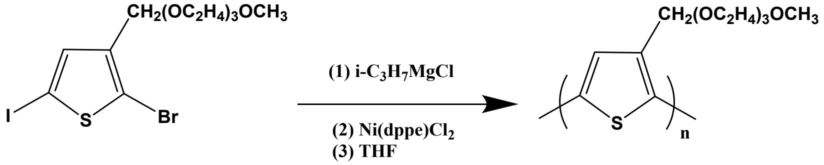

Scheme 1 The synthetic route of the P3EOT

The polymerization of 2-Bromo-5-iodo-3-(2-(2-(2-methoxyethoxy)ethoxy)ethoxy)methylthiophene was achieved by reacting of the monomer (932 mg, 2.00 mmol) with 1.0 mL isopropylmagnesium chloride (Aldrich, 2.0 M solution in THF) at 0^{o}C for 1 h under inert atmosphere. Then a mixture (suspension) of Ni (dppe) Cl2 (10.8 mg, 0.02 mmol, 1.0 mol%) in THF (12.0 mL) was added viaa syringe at 0^{O}C. After the reaction, mixture was stirred at 0^{o}C for additional 2 h, and then 5 M HCl was used to quench the polymerization. The crude product was run through a short silica gel column followed by soxhlet extraction using methanol, hexanes and THF. The final polymer P3EOT was obtained from THF fraction (310 mg, 61%). 1H-NMR (500 MHz, $CDCl_3$) d7.18 (s, 1H), 4.50 (s, 2H), 3.40-3.80 (m, 6H), 3.20 (s, 3H). 13C NMR (125 MHz,$CDCl_3$) d: 67.9, 69.9-71.6 (6 peaks) 130.2, 141.7, 136.1, 124.5 ppm. Glass transition temperature (Tg):-17^{o}C.

3. Transmission electron microscopy (TEM) imaging and analysis

Transmission electron microscopy was obtained on Zeiss LIBRA 120 operated at 120 kV acceleration voltage at Center for Nanophase Materials Sciences at Oak Ridge National Laboratory. A droplet of sample solution (4μL) was cast on copper grids (300 mesh, carbon film supported) and dried under ambient condition before TEM imaging.

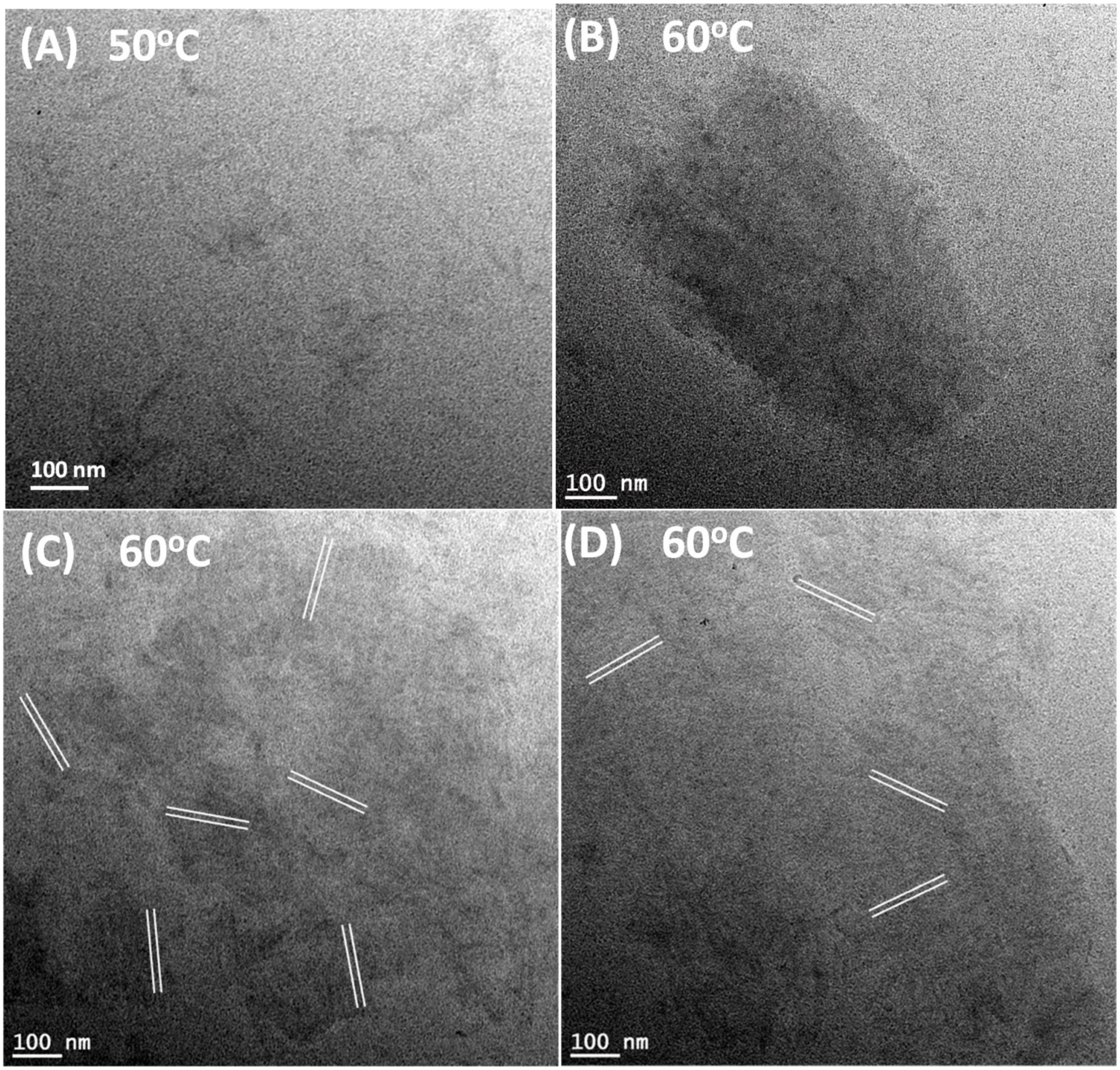

Figure S3. TEM images shows crystalline assemblies of P3EOT in D_2O at 50^oC (A) and 60^oC (B, C, D). The paralleled lines suggest possible lamellar stacking (001) of the nanowires.

TEM grids were prepared *via* drop-casting and solvent evaporation from P3EOT/D_2O solution at constant 50^oC or 60^OC. Mostly isolated one dimensional aggregates were observed at 50^oC, while larger three dimensional aggregates were found at 60^oC. The white lines highlight the possible (001) stacking regions in aggregates at 60^oC with a 15-20nm spacing. Those stacking regions are hundreds-nanometer long and possess different orientation.

4. Small angle x-ray and neutron scattering measurement

4.1 Small-angle x-ray scattering (SAXS)

SAXS experiments were conducted at DND-CAT at Advanced Photon Source at Argonne National Laboratory. X-rays of wavelength λ=0.73Å were used, and each measurements was performed at three different sample-to-detector distances (=0.2, 1.0, and 7.5 m) to cover an q-range of $0.0026 < q < 4.4$ Å-1, where $q = (4\pi/\lambda) \sin(\theta/2)$ is the magnitude of the scattering vector, and θ is the scattering angle. Our samples were prepared by dissolving the synthesized P3EOT into D_2O and $C_{12}E_5/D_2O$ (40 surfactant-wt%) and were measured in 1mm quartz capillary tubes at a wide range of temperature ($2 < T < 80$°C) as shown in **Figure 2.A** and **Figure S4**, in order to investigate the P3EOT chain conformation and morphology upon the temperature control as well as the surfactant/water phase transitions (hexagonal→micellar→lamellar phases, **Figure S4.A**).

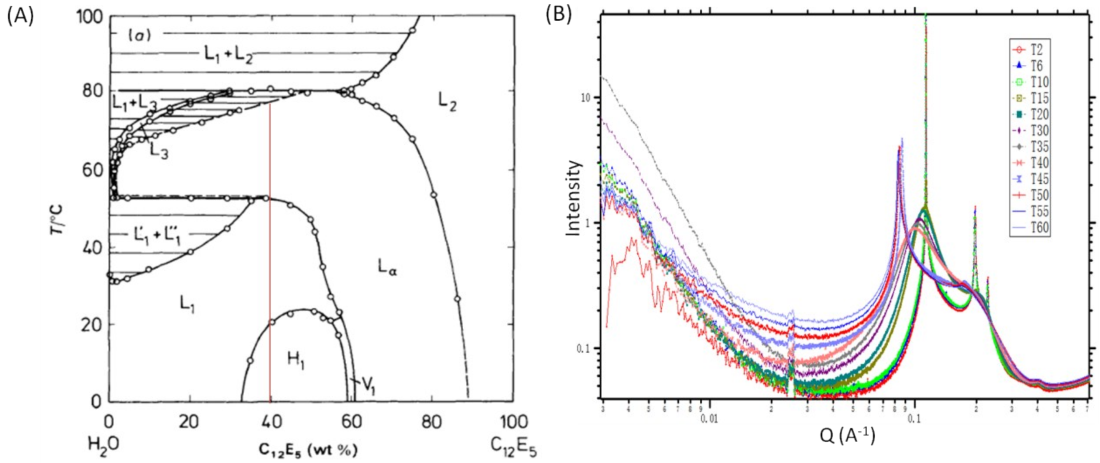

Figure S4. (A) Phase diagram of $C_{12}E_5$ aqueous solution. Red line at a 40wt% $C_{12}E_5$ concentration shows the thermal track studied in this paper, reproduced from [R. Strey, et al. Dilute Lamellar and L_3 Phases in the Binary Water-$C_{12}E_5$ System, J. Chem. Soc., Faraday Trans., 1990,86, 2253-2261]. (B) Small angle x-ray scattering profile of $C_{12}E_5$/D2O solution at a surfactant concentration of 40wt% from 2 to 60°C.

4.2 Guinier-Porod model and parallelepiped model for fitting SAXS data

As shown in Fig.2 (A), the scattering intensities I(q) at low temperature ($\leq 30°\mathrm{C}$) are from the isolated chain polymer contribution. At first, to model-independently obtain the structural information of isolated polymers in this region, our data were fitted by using the modified Guinier-Porod model, in which an intermediate Guinier region is included [7]:

$$I(q) = \frac{G_2}{q^{s_2}} e^{\left(\frac{-q^2 R_{g2}^2}{3-s_2}\right)} \quad \text{for } q \leq q_2,$$

$$I(q) = \frac{G_1}{q^{s_1}} e^{\left(\frac{-q^2 R_{g1}^2}{3-s_1}\right)} \quad \text{for } q_2 \leq q \leq q_1,$$

$$I(q) = \frac{D}{q^d} \quad \text{for } q_1 \leq q,$$

where *I(q)* is the scattering intensity at *q*, $3-s_1$ and $3-s_2$ are the dimensionality parameters (s = 0 for globular objects; 1 for rods; 2 for plates), R_{g1} and R_{g2} are the radii of gyration for small and overall sizes of scattering objects, and *G* and *D* are the scale factors. The fitted curves are presented by black dashed-lines in **Figure 2.A**, and the fitted parameters are shown in **Table S1**.

As temperature increases higher than 30°C, the polymers start to form aggregates and the growth of aggregates leads the increase of low-q intensity. In this temperature region ($35 \leq T \leq 45°\mathrm{C}$), isolated chains and polymer aggregates co-exist in the solution, and thus, both contributions from chains and aggregates should be considered in the model fitting analysis. We added two generalized Guinier-Porod models [7], which represent the contribution from chains and aggregates, by assuming that two components can be linearly summed to the total intensity without interparticle terms because of the low concentration of polymers in our aqueous solutions. The fitted results are presented in **Table S1**.

Table S1. Fitting results from SAXS intensities of P3EOT in aqueous solutions at T = 10-45°C

The modified GP model

Temperature (°C)	Dimensional parameter, s1	Radius of gyration for small size, Rg1 (A)	Dimensional parameter, s2	Radius of gyration for overall size, Rg2 (A)
10	0.41 ± 0.06	11.0± 1.3	0 ± 0.0015	28.6 ± 3.4
15	0.45 ± 0.05	11.0 ± 1.2	0 ± 0.0022	32.4 ± 2.3
20	0.49 ± 0.05	11.1 ± 1.0	0 ± 0.0024	33.6 ± 3.4
25	0.54 ± 0.04	11.0 ± 0.3	0 ± 0.15	36.0 ± 9.6
30	0.70 ± 0.05	10.7 ± 1.2	0 ± 0.0022	37.2 ± 2.3

Sum of two GP models					
Temperature (°C)	Volume ratio aggregate/coil	s1	Rg1 (A)	Dimensional parameter for aggregate	Rg2 (A)
35	2	0.73 ± 0.02	10.7 ± 0.3	1.19	496
40	4.5	0.55 ± 0.03	10.0 ± 0.4	1.44	711
45	10	0.32 ± 0.05	8.6 ± 0.8	1.61	987

Parallelepiped model				
Temperature (°C)	Width, W (A)	Thickness, t (A)	Aspect ratio W/t	Length, L (A)
20	21.0 ± 1.9	17.3 ± 1.7	1.21 ± 0.16	79.0 ± 2.5
25	20.5 ± 2.9	18.2 ± 2.8	1.12 ± 0.11	91.6 ± 2.9
30	21.3 ± 2.6	18.7 ± 2.4	1.14 ± 0.14	114.2 ± 3.6
35	26.5 ± 0.9	14.5 ± 0.7	1.82 ± 0.16	155.3 ± 9.7

In addition to such model-independent analysis, the parallelepiped model fitting is considered to obtain more detailed information about the chain conformations. Our optical measurements indicate that the initiation and growth of aggregates originates from the inter-chain π- π stacking, and the parallelepiped model analysis is one way to demonstrate how the cross-sectional shape of polymers changes during such stacking. The scattering intensity of randomly oriented parallelepipes with the thickness *t*, width *W*, and length *L* is given by [8],

$$I(q) = nV^2 \Delta\beta^2 \int_0^1 \phi\left(\mu\sqrt{1 - \sigma^2}, a\right) S^2(\mu c \sigma/2) d\sigma \quad ,$$

$$\phi(\mu, a) = \int_0^1 S^2\left(\frac{\mu}{2}\cos\left(\frac{\pi}{2}u\right)\right) S^2\left(\frac{\mu a}{2}\cos\left(\frac{\pi}{2}u\right)\right) du \quad ,$$

where the function S(x) is defined as sin(x)/x, n is the number density of objects, V and $\Delta\beta$ are the object volume and the scattering length density contrast in solutions (6.7×10^{-7}Å^{-2} by calculation), μ = qW, and a and c are the thickness and length normalized by W (t/W and L/W, respectively). The fitting results are shown in **Figure 2.C** and **Table S1**.

4.3 P3EOT contribution extracted from SAXS intensities of samples

For the cases where P3EOT polymers are dispersed in $C_{12}E_5/D_2O$ mixtures, our SAXS data show that the existence of P3EOT does not disturb the overall architecture of the hexagonal, micellar, and lamellar phases of $C_{12}E_5/D_2O$ systems. Yet, it is still not observed how these surfactant phases affect the polymer conformation or morphology. We directly extract the P3EOT contributions from P3EOT/D_2O solutions and P3EOT/$C_{12}E_5/D_2O$ solutions, and compare these two profiles to figure out the difference of polymer structures in the presence of surfactants. In the cases of the P3EOT/D_2O systems, the D_2O background is subtracted by assuming that the solvent contribution can be considered as a constant intensity in the range of 0.007 < q < 0.35 Å-1. In the case of P3EOT/$C_{12}E_5/D_2O$ systems, the $C_{12}E_5/D_2O$ SAXS intensity is subtracted from the P3EOT/$C_{12}E_5/D_2O$ intensity. As shown in the inset of Figure 4.(A), the P3EOT intensity exhibit q^{-1} behavior at 10°C, which implies that the polymers have rod-like elongated shapes contrary to the P3EOT in aqueous solutions. This P3EOT contribution in the hexagonal phase is fitted to parallelepiped model giving rise to a chain conformation of approximately 1.6nm, 2.4nm and 20nm in thickness, width and length, respectively (in **Table S2**). Even though there is a large fitting deviation, it may originate from the inter-polymer structure factors, i.e. peaks corresponding to the hexagonal periodicity, and it rather can suggest that under the confinement of hydrophilic domains in surfactant hexagonal phase, the initially coiled P3EOT chains are elongated and planarized. The contribution of P3EOT in a $C_{12}E_5$ micellar phase at 40°C shows the lower scattering intensity at low-q region compared to that in D_2O at the same temperature, and it may indicate an impeded growth of P3EOT aggregates by the concentrated micelles of $C_{12}E_5$. At last, the increased intensity at low-q region in the P3EOT contribution at 60°C implies that the large aggregates of P3EOT are formed in the $C_{12}E_5$ lamellar phase, but an absence of the P3EOT (100) diffraction peak shows that there is no side-by-side stacking of P3EOT.

Table S2. Fitting results for P3EOT contribution in $C_{12}E_5/D_2O$ hexagonal phase at T = 10°C

Parallelepiped model				
Temperature (°C)	Width, W (A)	Thickness, t (A)	Length, L (A)	SLD contrast (A-2)
10	24.3 ± 3.0	15.7 ± 1.8	198.6 ± 16.0	6.7e-7 (fixed)

4.4 (010) diffraction and solvent scattering in wide-angle x-ray scattering

While the (100) diffraction peak of P3EOT crystalline aggregates has been observed by SAXS in **Figure 2D**, the (010) peak due to π–π stacking of the polythiophene backbones is expected at q = 1.65A for a distance of 3.8nm in the x-ray scattering profile. As shown in **Figure S5**, we observed strong scattering intensity from the solvent (the hydrogen bonding structures of water molecules) at high-q region. There is no clear (010) peak found in the x-ray scattering profiles of P3EOT/D_2O solutions at 30-70^oC.

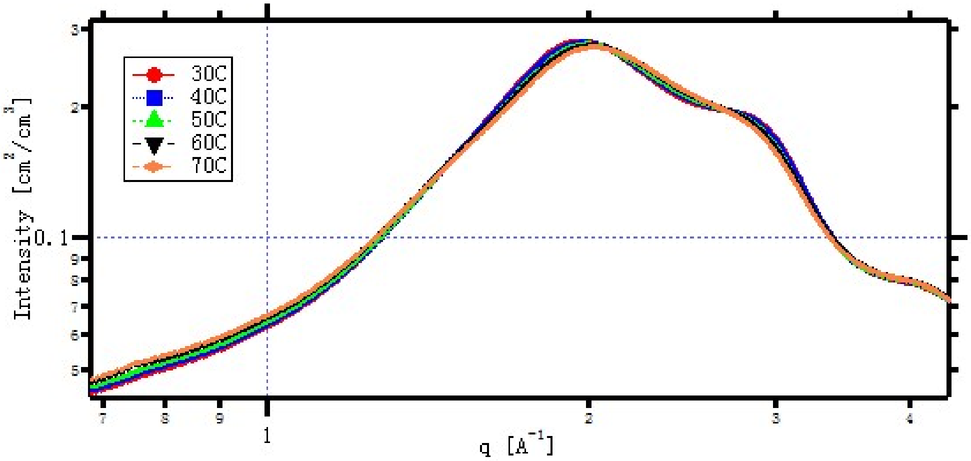

Figure S5. High-q region X-ray scattering profiles of P3EOT/D_2O solutions at 30 to 70^oC.

4.5 Small-angle neutron scattering (SANS) and model fitting results

Small angle neutron scattering (SANS) was measured at EQ-SANS at Spallation Neutron Source at Oak Ridge National Laboratory. Neutrons of wavelength λ = 2.5 and 9.5Å were used at two different sample-to-detector distances (= 1.3 and 4.0 m) to cover a q-range of 0.0099 < q < 0.5 Å-1. At first, we measured P3EOT/D_2O solutions at different temperatures (10-60°C) as presented in **Figure S6**. The initiation and growth of aggregates are observed, but due to the resolution and range of SANS measurements, we cannot observe (100) peaks or any transition at 35°C in our results, which is due to the slow data collection that lower the resolution to the periodic structure and transition kinetics.

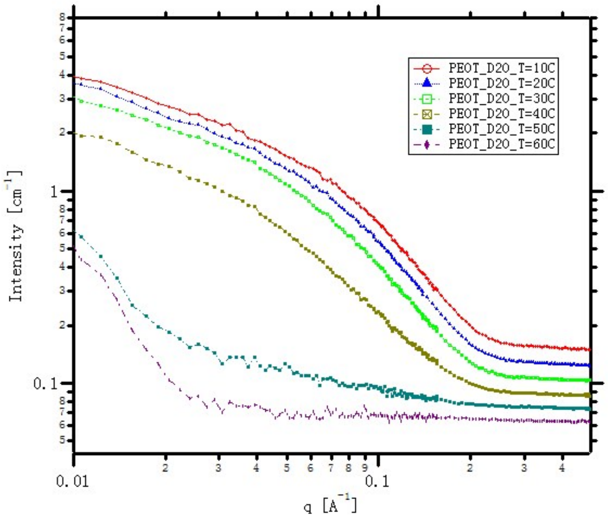

Figure S6. EQ-SANS results of P3EOT/D_2O. No (100) diffraction peak was observed.

At second, to confirm the lamellar phases of $C_{12}E_5$/D_2O samples and investigate the structure of lamellae, we measured the SANS intensity of $C_{12}E_5$/D_2O samples at 60°C with three $C_{12}E_5$ concentrations. It is known that the $C_{12}E_5$ molecules form bilayers, which are units of the lamellar structure in the given conditions as presented in **Figure S4.A** [9]. However, our system is a bulk system and, thus, long-range order between lamellae may be supposed to be suppressed because the system may prefer to form the distorted lamellar phase or sponge-like phase. In this fitting analysis, we assumed that $C_{12}E_5$ forms bilayer locally, but exhibits no long-range order in bulk system, and this assumption is quite agreed with the SANS data where the second lamellar peak is too weak to be clearly appeared. The scattering data were modeled by the form factor of randomly oriented disks and the structure factor with an in-out correlation factor as well as a lamellae-lamellae correlation factor [10, 11], which is given by,

$$I(q) = NP(q)S(q) + I_{bkg},$$

$$P(q) = \left(\pi\sigma^2\Delta\rho\right)^2 \frac{4\left\{1 - \cos\left(qt_{tail}\right)e^{-\frac{q^2\delta^2}{2}}\right\}}{q^2\left(q^2\sigma^2 + 2e^{-\frac{q^2\sigma^2}{6}}\right)}, \quad S(q) = 1 + \frac{A}{q}\tan^{-1}\left(\frac{q\xi_{io}}{2}\right) + \frac{B}{1 + \left(q - q_c\right)^2\xi^2},$$

where N is the number density that related with the full bilayer thickness, σ is the RMS radius of disks, $\Delta\rho$ is the scattering length density (SLD) contrast between bilayers and solvent, t_{tail} is the thickness of water-excluded hydrophobic layer of $C_{12}E_5$, δ is the RMS fluctuation of bilyers, A and B are the coefficients, ξ_{io} is the in-out correlation length, ξ is the bilayer-to-bilayer correlation length, q_c is $2\pi/D$ where D is the average bilayer-bilayer distance, and I_{bkg} is the incoherent scattering intensity. In this model fitting, we assumed that there is no significant change on the layer thickness by varying the $C_{12}E_5$ fraction, water molecules cannot penetrate the hydrophobic layer, SLD contrasts for hydrophobic layer (non-polar part of $C_{12}E_5$) and hydrophilic layer (polar part of $C_{12}E_5$+ water) are constant.

Additionally, we added P3EO$_4$T, whose side chains have one more ethylene oxide unit, into $C_{12}E_5/D_2O$ systems with 10 wt%. Based on the SAXS scattering intensities, we assumed that the addition of this conjugated polymer does not disturb the lamellar structure of $C_{12}E_5/D_2O$, and thus we fixed the layer thickness and the SLD of hydrophobic layer. P3EO4T can stay at the water layer between $C_{12}E_5$ layers, so the SLD of water layer was regarded as a free parameter. From the fitting results, we can confirm that our assumption for the layer thickness and no long-range order in lamellar structure is valid, and the existence of conjugated polymers does not significantly affect the lamellar structure (**Table S3**). Furthermore, the reduced SLD value of water layer can support our suggestion that conjugated polymers stay in the water layer, and we can estimate that the amount of polymer inside of water layers is approximately a half of added polymers, based on the SLD difference of water layer (6.33e-06 → 6.06e-06).

Table S3. Model fitting results for SANS measurements of $C_{12}E_5/D_2O$ and P3EO$_4$T/$C_{12}E_5/D_2O$ with $C_{12}E_5$ wt% = 20, 30, and 40. Polymer concentration is 10 wt%

	$C_{12}E_5$ (wt%)	**Tail layer thickness, t_{tail}(Å)	Spacing, D (Å)	Correlation length, ξ(Å)	Disk radius, σ(Å)	Fluctuation in layer thickness, δ (Å)
C12E5 /D2O	20	24.1	102.4	52.3	15.7	5.8
	30		97.3	62.4	12.3	5.0
	40		73.7	123.4	7.0	4.2
C12E5 /D2O /P3EO4T	20		103.1	75.5	18.6	7.0
	30		93.3	90.1	15.5	5.6
	40		71.5	144.9	7.5	4.4

$*\rho_{D2O} = 6.33 \times 10^{-6}\text{Å}^{-2}, \rho_{tail} = -0.40 \times 10^{-6}\text{Å}^{-2}$ (fixed) ** Linked during fitting

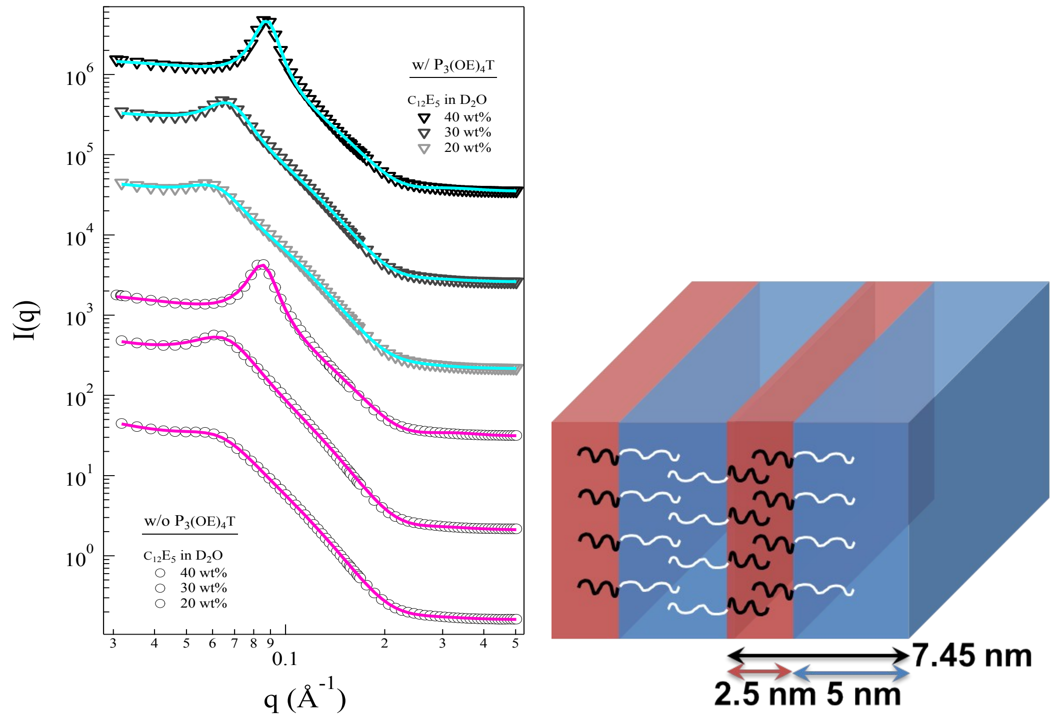

Figure S7. Small angle neutron scattering profile of both $C_{12}E_5/D_2O$ and P3EOT/$C_{12}E_5/D_2O$ systems at surfactant concentrations of 20wt%, 30wt% and 40wt%. P3EOT polymer concentration is 10 wt%.

5. Optical absorption and emission

UV-Vis absorption spectra were recorded using a Cary 5000 spectrometer from the sample solution. Photoluminescence was measured using a FluoroLog 3T fluorescence spectrometer excited with 450 nm light. Sample solution is prepared at a 0.05 wt.% P3EOT concentration.

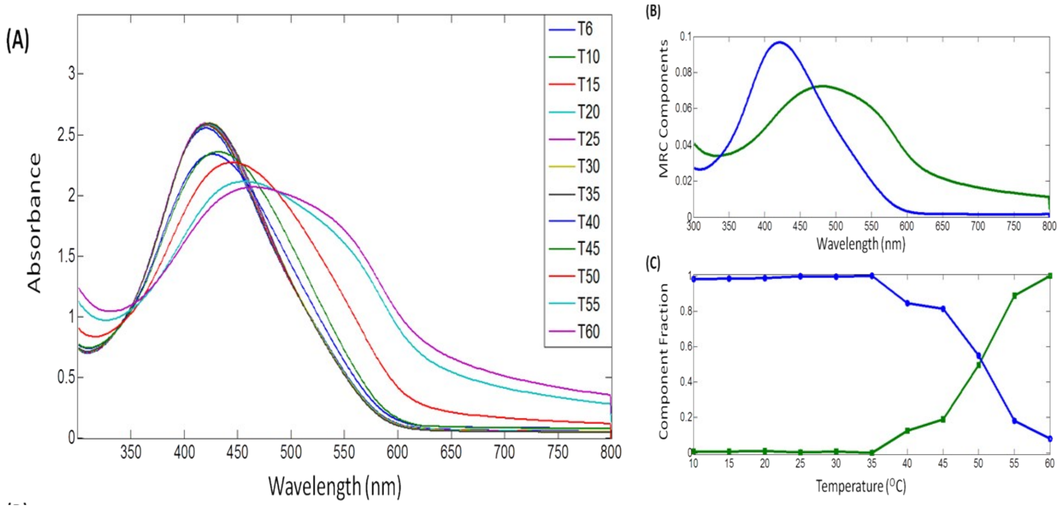

Figure S8. Thermo-chromic behavior of P3EOT/$C_{12}E_5/D_2O$ solution. (A) UV-vis absorption spectra of P3EOT/$C_{12}E_5/D_2O$ solution at 6-60^{O}C. (B) Two major components were deconvoluted by multivariate curve resolution (MCR) analysis of the absorption spectra. (C) Changes in the fraction of the two components in each absorption spectrum as a function of temperature derived from the MCR analysis.

6. ^{1}H-NMR analysis

Variable temperature proton NMR analyses on a sample of P3EOT in D_2O were performed over the temperature range 22.9 ^{O}C to 70.3 ^{O}C (and then cycled back down to 22.9 ^{O}C) on a Varian VNMRS 500 spectrometer, operating at 499.716 MHz for proton. Prior to the VT experiment, the OneNMR probe temperatures were calibrated over this range using the separation between the methylene and hydroxyl peaks (Δppm) of 100% ethylene glycol (sealed standard sample) using the relationship T(K) = (4.637-Δppm)/0.009967 in the usual manner[13a]. The accuracy using ethylene glycol is generally within ±0.5 ^{O}C.[13b] Spectra were recorded (acquisitions started) at 15 min and 30 min after the probe had reached the desired temperature. Spectra were obtained using nitrogen flow gas at the following temperatures in ^{O}C (actual temperatures based on the probe calibration): 22.9, 30.2, 35.5, 39.7, 45.0, 50.3, 54.5, 59.7, 65.0, 70.3, 65.0, 59.7, 54.5, 50.3, 45.0, 39.7, 35.5, 30.2, 22.9, with a final spectrum taken at 22.9 ºC after sitting for 15.5 hrs. Acquisition parameters included a recycle delay of 3 sec, an acquisition time of 1.638 sec, with 32 transients and a sweep width of 6009.6 Hz. Chemical shifts were referenced to the DHO peak residue, set to 4.80 ppm.

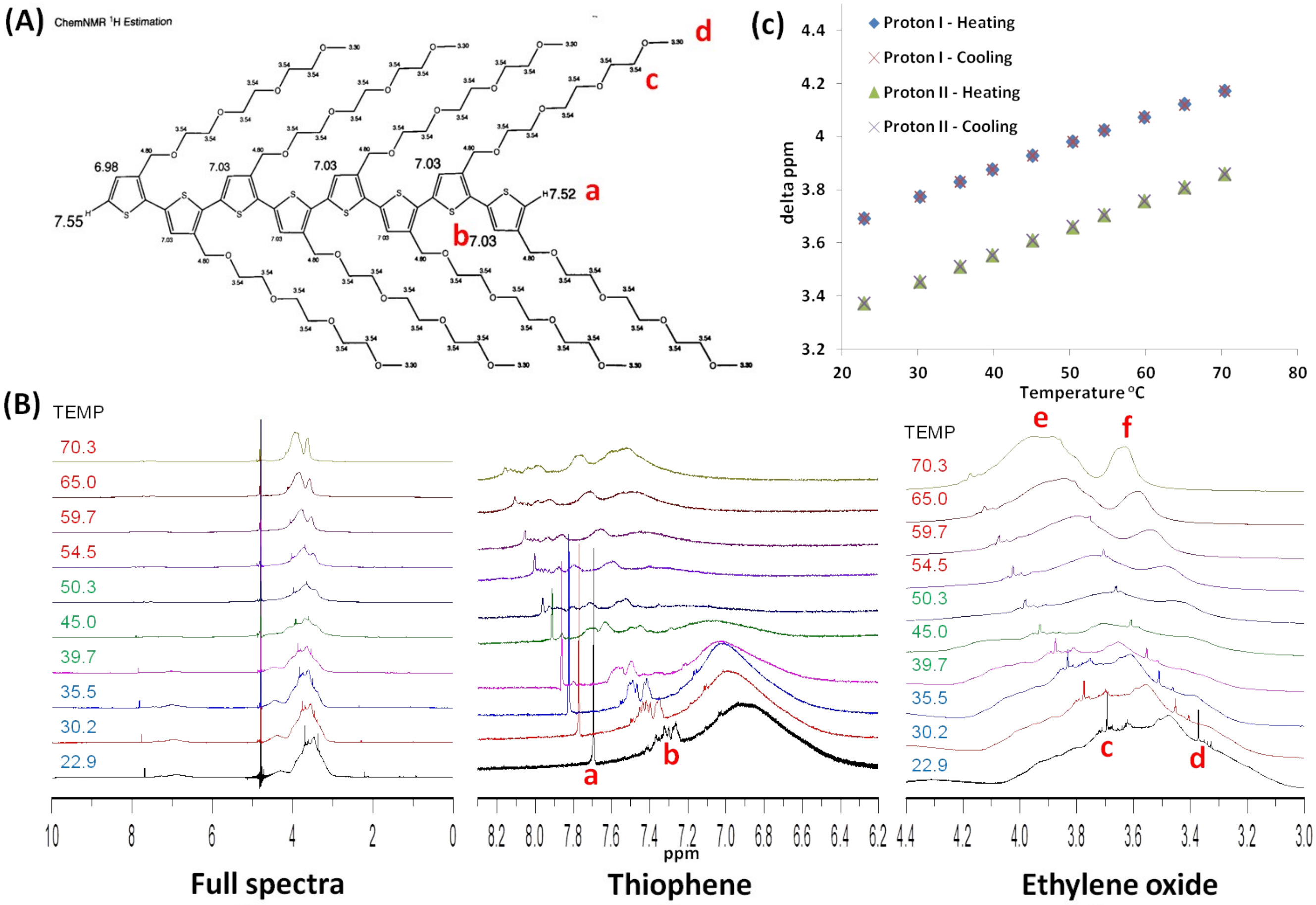

Figure S9. (A) Chemical structure of P3EOT and ^{1}H resonance peak estimation. (B) ^{1}H NMR spectra of P3EOT solution on a heating trace from 22.9 to 70.3°C. Peak regions from protons of thiophene backbone and ethylene oxide side chains are highlighted. (C) ^{1}H NMR peak shifts of proton ***c*** (proton I) and ***d*** (proton II) from ethylene oxide side chains upon thermal control.

We observed side chain conformational evolution from 1H-NMR measurement in **Figure S9**. Sharp resonance peaks **c** and **d** from mid and chain-end protons in ethylene oxide chains were resolved at 23 °C when polymer adopts a coil-chain conformation at room temperature. Upon increasing temperature, both peaks shifted downfield (**Figure S9.C**), which is probably due to the decreased solubility of ethylene oxide chains and smooth changes in ether-water hydrogen bonding. The peak intensity, however, showed a sharp decrease after 35.5°C, which is close to the early aggregation temperature observed in SAXS and UV-Vis spectroscopy, demonstrating the collapse of ethylene oxide chains. Two new broad peaks, **e** and **f**, raised after heating to 50.3°C, which is close to the temperature of side-by-side ordering, probably due to the additional interaction (i.e. hydrogen bonding) between ethylene oxide chains from neighboring P3EOT molecules at [100] direction. However, our X-ray results do not show changes in side chain stacking distance as a function of temperature at 55 to 75°C, suggesting minimum effect of side chain collapse on structure of highly ordered aggregates.

7. Thermal reversibility of conformational changes

The transition between the thermodynamically stable states, such as coiled or planarized chains, is expected to be reversible. However, due to the relatively large molecular weight of conjugated polymers like P3EOT, the conformational evolution as well as the aggregation process of polymer chains is very slow process. A quantitatively study on the coil-aggregate transition kinetics during heating and cooling trace has been performed using MCR analysis on the UV-VIS-NIR absorption spectra (the absorption in the near-IR regions is mainly attributed to the solvent, water). As shown in the **Figure S10**, the aggregate-to-coil transition during cooling mainly occurs at 55^{O}C-40^{O}C. We stabilized the P3EOT solution for 30min between advancing temperature 10^{O}C higher or lower. However, the results of the MCR analysis shows that the yield of coil chains is smaller compared to that at the same temperature of heating trace. After cooling back to 20^{O}C and annealed for 0.5h, we recovered only 80% of P3EOT chains to coiled conformations. The rest of the P3EOT, 20% chains, exist in the aggregates likely adopting planarized conformation. Due to the relatively slow chain conformational dynamics, P3EOT becomes fully dissolved after 24 hours annealing to generate the absorption spectrum showing 100% coiled component.

We applied a similar 30 min thermal stabilization for the SAXS sample solutions at different temperatures. Due to the limited beam time we acquired data during heating.

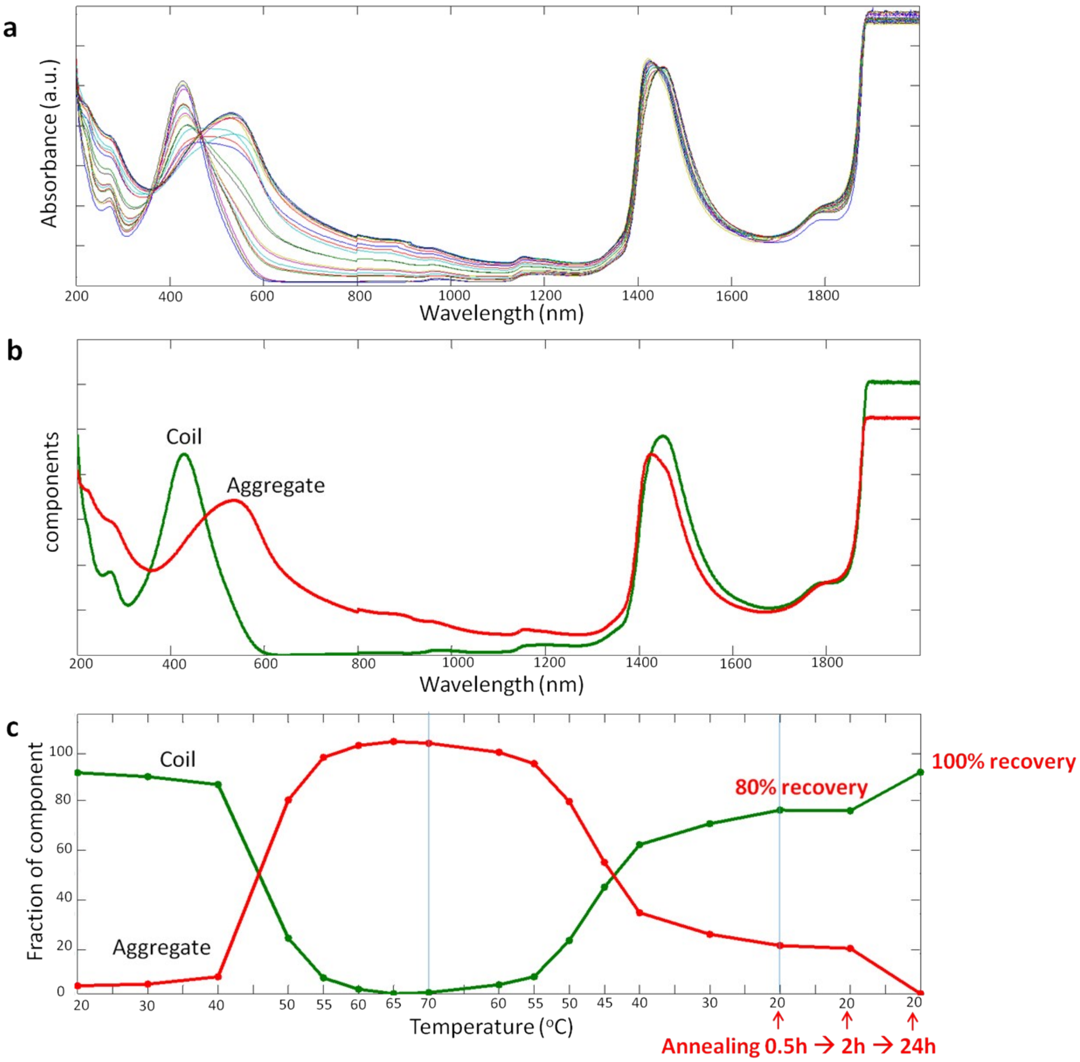

Figure S10. a) UV-VIS-NIR absorption spectra of P3EOT aqueous solution during heating and cooling between 10 to 70^{o}C. The spectrum was measured after 30 min thermal stabilization at each temperature. After the thermal cycle was finished, the P3EOT solution was equilibrated at 20^{o}C for 24h. b) Two spectra corresponding to coils and aggregates of P3EOT are deconvoluted by MCR analysis from original data (Fig.1a) c) The changes in component concentration of coil and aggregate component (MCR fit results) solution during the thermal cycle and further thermal equilibration.

References

1. Matsen, M. W. Journal of Physics-Condensed Matter 2002, 14, 21-47
2. Matsen M. W.; Schick M. Current Opinion in Colloid and Interface Science 1996, 1, 329-336.
3. Fredrickson, G.H., The Equilibrium Theory of Inhomogeneous Polymers (Clarendon Press, Oxford, 2006).
4. Sides, S. W.; Fredrickson, G. H. Polymer 2003, 44, 5859−5866.
5. de Gennes, P.G, Scaling Concepts in Polymer Physics (Cornell University Press, New York, 1979).
6. Warner, M.; Gunn, J.M.F.; Baumgartner, A.B., J. Phys. A: Math. Gen. 1985, 18, 3007-3026.
7. B. Hammouda, A new Guinier-Porod model, J. Appl. Cryst. 2010, 43:716-719
8. Mittelbach and Porod, Acta Physica Austriaca, 1961, 14
9. R. Strey, et al. Dilute Lamellar and L3 Phases in the Binary Water-C12E5 System, J. Chem. Soc. Faraday Trans. 1990, 86(12)
10. N. Lei, et al, Synchrotron x-ray-scattering studies on the sodium dodecyl sulfate–water–pentanol–dodecane L3 sponge phase, Phys. Rev. E, 1997, 56
11. L.Porcar, et al, Scaling of Structural and Rheological Response of L3 Sponge Phases in the "Sweetened" Cetylpyridinium/Hexanol/Dextrose/Brine System, Langmuir, 2003, 19
12. T. Higashihara, et al. Synthesis and characterization of block copolythiophene with hexyl and triethylene glycol side chains. Polymer. 2011, 52, 3687-3695.
13. (a) See for example M. J. Wiester et al. Solvent and temperature Induced Switching Between Structural Isomers of Rh(I) Phosphinoalkyl Thiother (PS) Complexes. Inorg. Chem. 2010, 49, 7188-7196. (b) W. M. Spees et al. Use of Ethylene Glycol to Evaluate Gradient Performance in Gradient-Intensive Diffusion MR Sequences. Magn. Reson. Med. 2012, 68, 319-324.